Benchmark calculations for electron collisions with zinc atoms

Oleg Zatsarinny* and Klaus Bartschat†
Department of Physics and Astronomy, Drake University, Des Moines, Iowa 50311, USA
(Received 26 October 2004; published 24 February 2005)

We present results from *R*-matrix (close-coupling) calculations for elastic scattering and electron impact excitation of Zn. The overall agreement between the predictions from two independent models, using either a semiempirical core potential or a recently developed *B*-spline approach with nonorthogonal orbitals, is very satisfactory. The latter method, however, yields particularly good agreement with the few existing experimental benchmark data for resonances at low incident energies.

DOI: 10.1103/PhysRevA.71.022716 PACS number(s): 34.80.Bm, 34.80.Dp

I. INTRODUCTION

Electron collisions with quasi-two-electron atoms are important for both fundamental and applied reasons. Over many years, collision models have been tested on helium, and the extension to targets such as Be, Ca, Zn, and even Hg was often achieved by representing the inner core electrons by a model potential. In light of modern computational resources, both hardware and software, low-energy electron collisions with such targets are sometimes viewed as not very challenging for theorists, since the close-coupling expansion is generally believed to be an ideal tool to obtain accurate results. For elastic scattering in particular, special methods such as the "polarized orbital approach" [1] are expected to be appropriate, since they can accurately represent exchange between the projectile electron and the target, as well as the polarization of the target due to the projectile.

In a recent paper on *e*-Mg collisions [2], however, we pointed out that the close-coupling expansion does not provide a straightforward way of systematically improving the calculation of low-energy resonances, due to the lack of a minimization principle relating the position of a shape or Feshbach resonance to the energy of the target state(s) with which the resonance is associated. Improving the quality of the models for both the target structure and the collision dynamics *does not guarantee* a concurrent improvement of the resonance description.

As mentioned above, low-energy electron collisions with quasi-two-electron atoms are of great practical interest, for instance in the modeling of discharges. Important examples include *e*-Hg collisions in mercury-based fluorescence lamps and *e*-Zn collisions, where Zn is used instead of Hg to reduce the possible environmental problems associated with mercury in lamps [3,4]. Due to the limited number of experimental studies, in particular the availability of *absolute* cross sections, modelers essentially have to rely on theory to provide the necessary input data for their simulations. Details of the data needs for *e*-Zn collisions and examples of the data use in modeling were recently discussed by White and collaborators [5]. In the latter work, some of the electron-impact excitation cross sections for *e*-Zn collisions presented in this paper were used, together with results for elastic scattering obtained by a polarized-orbital approach, similar to that described by McEachran and Elford [6]. Note, however, that there was a major discrepancy between the calculated low-energy dependence of the elastic cross section and the available experimental evidence, particularly the work of Burrow and collaborators [7], which was recently extended by Sullivan *et al.* [8].

In light of this controversy in the low-energy purely elastic regime, and the need for accurate cross-section data for electron-impact excitation, we applied two *R*-matrix (close-coupling) models to the *e*-Zn collision problem. One set of results was obtained with the well-known suite of Belfast codes [9], while the other set was generated using a *B*-spline implementation, which also allows for the use of term-dependent and, therefore, nonorthogonal target orbitals. The latter method, described in detail by Zatsarinny and Froese Fischer [10], is under further development in our group and was applied very successfully to the *e*-Mg collision problem mentioned above, as well as to electron collisions with heavy noble gases such as neon [11,12] and argon [13].

This paper is organized as follows: After discussing the description of the target structure in both approaches, we summarize the most important aspects of the collision calculations. This is followed by a presentation of the cross sections for the most important transitions starting with Zn in its ground state. Finally, a detailed discussion of the various low-energy resonance features is provided, and the results are compared with the available experimental information.

II. NUMERICAL METHODS

This section describes the two methods used for the structure and collision calculations. We start with a brief description of a core-potential approach before focusing on the *B*-spline *R*-matrix (BSRM) method. As mentioned above, the latter also allows for term-dependent, nonorthogonal orbitals in the target description. This high flexibility is very advantageous in the low-energy near-threshold resonance regime, on which we concentrate in the current work.

A. Structure calculations

Zinc, with the ground state configuration $[1s^2 \ldots 3d^{10}](4s^2)\,^1S$ and singly-excited states $[1s^2 \ldots 3d^{10}]$

*Electronic address: oleg_zoi@yahoo.com
†Electronic address: klaus.bartschat@drake.edu

$\times(4sn\ell)^{3,1}L$ (where $L=\ell$) exhibits many similarities to helium, i.e., it can sometimes be viewed as two electrons outside of a doubly ionized core. For simplicity, closed shells will be omitted in the notation below.

1. The core potential approach

The target states were constructed by adding semiempirical exchange and polarization potentials to the Hartree potential of the Zn^{2+} core to ensure very good agreement (better than 0.2% for all members of the *S*, *P*, *D*, and *F* Rydberg series up to $n=9$) of the ionization potentials of the various Zn^+ states with the experimental data [14]. This was achieved by using the program COREPOT of Bartschat [15]. The target states of neutral zinc were then constructed as multiconfiguration expansions of the form $3d^{10}n\ell n'\ell'$ with $n\ell$, $n'\ell'$ including 4*s*, 4*p*, 4*d*, 5*s*, 5*p*, 5*d*, 6*s*, 6*p*, and 6*d*.

This approach, based on the ionic orbitals, is known to generally yield a good description of the states for the neutral atom as well, provided a sufficient amount of configuration interaction is included. In the present work, the excitation energies of the lowest eight states from the ground state of Zn were accurate to about 0.2 eV, i.e., at the 5% level compared to experiment [14]. Although it is certainly acceptable, this target description cannot really compete with the 1% accuracy level achieved with the nonorthogonal method described below. The oscillator strengths for the $(4s^2)^1S \rightarrow (4s4p)^1P^o$ and $(4s^2)^1S \rightarrow (4s5p)^1P^o$ transitions were obtained as 1.649 and 0.328, respectively, and the static dipole polarizability as 41 a_0^3 (where $a_0=0.529\times10^{-10}$ m is the Bohr radius). These results are again in satisfactory agreement with experiment [16,17] (see also Table II), but they are not as accurate as those obtained with nonorthogonal orbitals.

2. The nonorthogonal orbital approach

Both valence and core-valence correlation are important for the ground state and the low-lying excited states of Zn. As mentioned above, a widely used method of incorporating core-valence correlation is based upon applying a semiempirical core-polarization potential. Although such a potential simplifies the calculations significantly and can provide accurate excitation energies and oscillator strengths, the question always remains how well the model potential can simulate *all* core-valence correlation, including nondipole contributions. In the present approach, we therefore chose to include the core-valence correlation *ab initio* by adding target configurations with an excited core. However, direct multiconfiguration Hartree-Fock (MCHF) calculations in this case usually lead to very large expansions, which can hardly be used in subsequent scattering calculations. For this reason, we used the *B*-spline box-based close-coupling method [18] to generate the target states. This method also provides a systematic way of constructing pseudostates, which are very important for the *e*-Zn collision problem in general.

Specifically, the calculation of the target states included the following steps. We started by generating the core orbitals from a Zn^{2+} Hartree-Fock calculation and then obtained valence 4*s*, 4*p*, 4*d*, and 5*s* orbitals from a frozen-core calculation for Zn^+. We then simulated the core-valence correlation by adding the $3d^9\overline{n\ell}\overline{n\ell}'$ configurations, where the bar indicates a correlated rather than a physical orbital. Different sets of correlated orbitals $\overline{n\ell}$ were optimized for each Zn^+ state separately. Since the mean radii for the $\overline{n\ell}$ orbitals lie between the mean radii of the core and the valence orbitals, this method allows us to incorporate the core-valence correlation with a relatively small number of configurations.

The core-valence correlated states of Zn^+ were then used as target states in *B*-spline bound-state close-coupling calculations to generate the low-lying states of atomic Zn. The corresponding close-coupling expansion had the structure

$$\begin{aligned}\Phi(3d^{10}3sn\ell,LS) = {}& \mathcal{A}\sum_i \{\phi(3d^{10}4s)P(n_i\ell_i)\}^{LS} \\ & + \mathcal{A}\sum_i \{\phi(3d^{10}4p)P(n_i\ell_i)\}^{LS} \\ & + \mathcal{A}\sum_i \{\phi(3d^{10}5s)P(n_i\ell_i)\}^{LS} \\ & + \mathcal{A}\sum_i \{\phi(3d^{10}4d)P(n_i\ell_i)\}^{LS} \\ & + \mathcal{A}\sum_i \{\phi(3d^{9}4s^2)P(n_i\ell_i)\}^{LS} \\ & + \sum_i \chi(3d^9n_i\ell_i\overline{n\ell}'\overline{n\ell}'',LS), \end{aligned} \tag{1}$$

where $\mathcal{A}$ denotes the antisymmetrization operator. Note that we also added the $3d^94s^2$ core-excited state of Zn^+. The unknown functions for the outer valence electron were expanded in the *B*-spline basis and the corresponding equations were solved subject to the condition that the wave functions vanish at the boundary. This scheme yields nonorthogonal, term-dependent orbitals for each *LS* term. The number of physical states which we can generate in this method depends on the size *a* of the *R*-matrix box. We chose $a=35a_0$, which allowed us to obtain a good description for all low-lying states of Zn up to $(4s6s)^1S$. Along with these physical states, we also generated a set of pseudostates for each symmetry, with the lowest states representing the remaining bound states and the others representing the continuum. Note that the pure close-coupling expansion exhibits a very slow convergence for the lowest bound state, such as the $(4s^2)^1S$ ground state in Zn, where short-range correlations are very important. For the $(4s^2)^1S$ state, we therefore used the direct MCHF expansion, with promotion of both valence and one core orbital. We included 67 *B*-splines of order 8 in the present calculations. Of course, since the above *B*-spline bound-state close-coupling calculations generate different nonorthogonal sets of orbitals for each atomic state, their subsequent use is somewhat complicated. On the other hand, our configuration expansions for the atomic target states only contain between 40 and 100 configurations for each state and hence can be used in the collision calculations with only modest computational resources.

The target states generated for the *B*-spline scattering calculations are given in Table I. We see good agreement with experiment for the excitation energies of the lowest 11 spec-

TABLE I. Target states of Zn used in the BSRM model. The last four states were included because of their relatively important contributions to the polarization of the ground state (see Table II).

State	Excitation energy (eV)	Experiment [14] (eV)	State	Excitation energy (eV)
Spectroscopic:			$(4sks)^3S$	9.559
$(4s^2)^1S$	0.000	0.000	$(4sks)^1S$	9.637
$(4s4p)^3P^o$	4.127	4.054	$(4skd)^1D$	9.708
$(4s4p)^1P^o$	5.839	5.796	$(4skd)^3D$	9.882
$(4s5s)^3S$	6.690	6.654	$(4skp)^3P^o$	9.978
$(4s5s)^1S$	6.931	6.917	$(4skp)^1P^o$	10.060
$(4s5p)^3P^o$	7.597	7.601	$(4p^2)^3P$	10.098
$(4s4d)^1D$	7.734	7.744	$(4sks)^3S$	10.641
$(4s4d)^3D$	7.776	7.783	$(4sks)^1S$	10.723
$(4s5p)^1P^o$	7.798	7.800	$(4skp)^1P^o$	11.167
$(4s6s)^3S$	8.109	8.113	$(4skd)^1D$	11.283
$(4s6s)^1S$	8.182	8.188	$(3d^94s^24p)^3P^o$	11.481
Pseudostates:			$(4p^2)^1S$	11.612
$(4s6p)^3P^o$	8.448		$(3d^94s^24p)^3F^o$	11.977
$(4s5d)^1D$	8.470		$(3d^94s^24p)^1P^o$	12.054
$(4s5d)^3D$	8.506		$(3d^94s^24p)^1F^o$	12.130
$(4s4f)^3F^o$	8.522		$(3d^94s^24p)^1D^o$	12.303
$(4s4f)^1F^o$	8.522		$(3d^94s^24p)^3D^o$	12.312
$(4s6p)^1P^o$	8.528		$(4skp)^1P^o$	12.475
$(4sns)^3S$	8.762		$(4skp)^1P^o$	12.951
$(4sns)^1S$	8.821		$(4p^2)^1D$	13.537
$(4snd)^1D$	9.009		$(3d^94s^25p)^1P^o$	15.345
$(4snd)^3D$	9.078		$(3d^94s^2kf)^1P^o$	28.807
$(4snp)^3P^o$	9.087		$(3d^94s^2kf)^1P^o$	31.327
$(4snp)^1P^o$	9.172		$(3d^94s^2kf)^1P^o$	34.061
Ionization limit		9.394	$(3d^94s^2kf)^1P^o$	37.006

troscopic states. The other target states represent the remaining bound states and the low-energy continuum. We also included the $3d \rightarrow 4p$ and $3d \rightarrow 4f$ core-excited states, which were found to be important scattering channels for the *e*-Zn collision problem. The pseudostates were chosen to guarantee a good representation of the polarizability of the ground state. The oscillator strengths for transitions from the ground state and the corresponding contributions to the polarizability are given in Table II. The oscillator strength for the resonance transition $(4s^2)^1S \rightarrow (4s4p)^1P^o$ obtained using the above method is close to the value recommended by NIST [17]. This transition provides the principal contribution to the polarizability of the ground state, with the $4s \rightarrow 5p$ and $3d \rightarrow 4p$ excitations also being somewhat important. The final value of the static dipole polarizability is close to the experimental data [16]. In fact, when all pseudostates generated in the *B*-spline box-based approach are included in the calculation, we obtain a value of 38.6 a_0^3. This is very close to experiment, but the remaining pseudostates contribute less than 0.05 a_0^3 each. Hence, we opted for the above model since it could still be handled on a desktop workstation.

Finally, we note that the experimental energy splittings for the spectroscopic states were used in the subsequent scatter-

TABLE II. Contributions to the polarizability of the Zn ground state in the BSRM model.

Upper level	Oscillator strength	Polarizability (a_0^3)	Experiment
$(4s4p)^1P^o$	1.450	31.952	1.468 [17]
$(4s5p)^1P^o$	0.095	1.155	
$(4s6p)^1P^o$	0.025	0.251	
$(4snp)^1P^o$	0.015	0.129	
$(4skp)^1P^o$	0.003	0.020	
$(4skp)^1P^o$	0.010	0.057	
$(3d^94s^24p)^1P^o$	0.450	2.289	
$(4skp)^1P^o$	0.035	0.165	
$(4skp)^1P^o$	0.037	0.165	
$(3d^94s^25p)^1P^o$	0.046	0.143	
$(3d^94s^2kf)^1P^o$	0.116	0.103	
$(3d^94s^2kf)^1P^o$	0.145	0.109	
$(3d^94s^2kf)^1P^o$	0.174	0.111	
$(3d^94s^2kf)^1P^o$	0.196	0.106	
Total		36.755	38.8 ± 0.8 [16]

ing calculations. This allows for a direct comparison between experiment and theory. In the standard *R*-matrix method, this is achieved by adjusting the so-called "continuum-continuum elements" of the Hamiltonian before diagonalization [9]. Note, however, that this procedure that can cause inconsistencies due to the lack of a general recipe for adjusting the "bound-bound elements." The latter part of the Hamiltonian matrix originates when the projectile orbitals are constructed orthogonal to the target orbitals. In the BSRM method, no such bound-bound block is required (see below), and hence the position of a resonance relative to its parent target state(s) is conserved even after adjusting the target thresholds.

B. Collision calculations

1. Standard R-matrix with core potential

The semirelativistic *R*-matrix code of Berrington *et al.* [9] was employed to perform the inner-region calculation. Using 25 numerical orbitals and a radius of $40a_0$ ensured that exchange effects between the projectile and the target electrons could be neglected outside the *R*-matrix sphere and that numerically reliable results for partial waves up to a total orbital angular momentum of $L=15$ could be generated for collision energies up to 20 eV. The calculation for the external region was performed using the flexible asymptotic *R*-matrix package FARM of Burke and Noble [19]. When necessary, results for the optically allowed $^1S \rightarrow {}^1P^o$ transitions included contributions from higher partial waves. These were generated by using a geometric extrapolation scheme. Altogether, 25 states were closely coupled in the above model, with the lowest nine $(4s n\ell)$ states being well-represented physical target states.

2. The B-spline R-matrix approach

For the alternative scattering calculations we employed the recently developed *B*-spline *R*-matrix code [10]. Details of this approach can be found, for example, in our recent publication on *e*-Mg collisions [2]. The distinctive feature of the method is the use of *B*-splines as a universal basis to represent the scattering orbitals in the inner region of $r \leqslant a$. Hence, the *R*-matrix expansion in this region takes the form

$$\Psi_k^\Gamma(x_1, \ldots, x_{N+1}) = \mathcal{A} \sum_{ij} \overline{\Phi}_i^\Gamma(x_1, \ldots, x_N; \hat{\mathbf{r}}_{N+1}\sigma_{N+1}) r_{N+1}^{-1} B_j(r_{N+1}) a_{ijk}^\Gamma, \qquad (2)$$

where the $\overline{\Phi}_i$ are the channel functions while the splines $B_j(r)$ represent the continuum orbitals. The principal advantage of *B*-splines is that they form an effectively complete basis, and hence no Buttle correction to the *R*-matrix is needed in this case. The amplitudes of the wavefunctions at the boundary, which are required for the evaluation of the *R*-matrix, correspond to the coefficient of the last spline, which is the only spline with nonzero value at the boundary.

The other important feature of the present code concerns the orthogonality requirements for the one-electron radial functions. As outlined above, we do not require any orthogonal conditions for the one-electron radial functions used to represent the target states, and the continuum orbitals do not have to be orthogonal to the bound orbitals either. The use of non-orthogonal orbitals allows us to avoid the introduction of additional $(N+1)$-electron terms in the *R*-matrix expansion. For practical reasons, however, we imposed limited orthogonality conditions on the scattering orbitals by forcing them to be orthogonal to the bound orbitals representing closed subshells. This is advantageous from a numerical point of view but otherwise has very little effect on the results.

The number of *B*-splines and the *R*-matrix radius in the scattering calculations were chosen the same as in the calculation of target bound states. We numerically calculated partial-wave contributions up to $L=12$. The cross-section calculations were then carried out in the same way as in the standard *R*-matrix calculations.

III. RESULTS AND DISCUSSION

A. Cross sections for *e*-Zn scattering

Figure 1 displays the electron transmission signal (ETS) for electron collisions with Zn atoms in their ground state $(4s^2)^1S$. After convolution of the raw theoretical results with the experimental energy resolution of 50 meV, there is excellent agreement between the experimental data of Burrow *et al.* [7] and the BSRM predictions for the energy derivative of the total cross section, which is proportional to the ETS. Several rapid variations of the signal are observed, particularly near the excitation thresholds. These will be further discussed below. Also shown are the predictions from the core-potential approach. While this method achieves qualitative agreement with experiment as well, the details are not predicted as well as they are in the BSRM calculation.

Figure 2 exhibits our predictions for the angle-integrated elastic cross section. Overall, there is very satisfactory agreement between the results from the corepotential and the BSRM approaches. One discrepancy occurs in the position and, consequently, the height of the first cross-section maximum below 1 eV. This sensitivity of the theoretical models is of the same nature as we observed in our recent work on *e*-Mg collisions [2]. However, our resonance position agrees much better with the experimental findings [7,20] than the polarized-orbital results presented and used by White *et al.* [5]. The other discrepancy concerns the energy region very close to the threshold of the $(4s4p)^3P^o$ state. Again, it is very difficult to theoretically predict the fine details of this resonance feature, since one can expect a high sensitivity of the results to the details of the model, particularly the relative position of the $(N+1)$-electron resonance and the *N*-electron target state.

Figures 3–6 present our low-energy results for electron-impact excitation of the $(4s4p)^{3,1}P^o$ and $(4s5s)^{3,1}S$ states. Once again, there is overall good agreement between the predictions from the two methods, with a notable exception in the vicinity of the $(4s4p)^3P^o$ threshold. Likely most important for modeling applications, however, is the large cross section predicted for excitation of the latter state for incident energies between 4 eV and 8 eV, which dominates the exci-

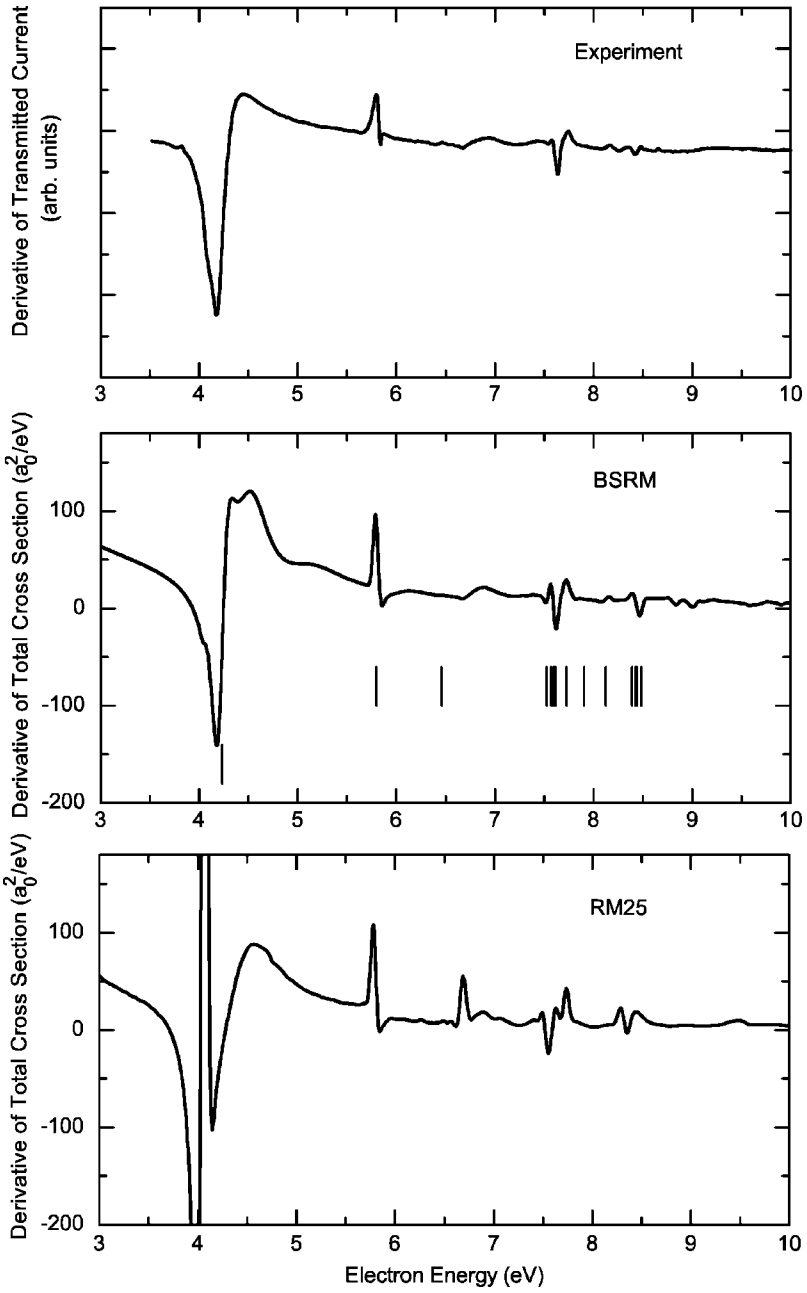

FIG. 1. Electron transmission signal for electron collisions with Zn atoms in their ground state $(4s^2)^1S$. The top panel presents the experimental signal obtained in the work described in [7], while the middle and bottom panels show the derivative (with respect to the energy) of the total cross section (units of a_0^2/eV) as obtained in the BSRM and the 25-state standard core-potential *R*-matrix (RM25) approaches. The theoretical results were convoluted with a Gaussian representing the experimental energy resolution of 50 meV (FWHM). The vertical lines in the BSRM panel represent the thresholds of the first eleven excited states.

tation of the other three states shown, including the optically allowed $(4s^2)^1S \rightarrow (4s4p)^1P^o$ transition.

Finally, Fig. 7 provides an overview of the largest cross sections for incident energies up to 50 eV. Due to the lack of coupling to the target continuum in the present BSRM calculation, we do not expect the predictions of the small cross sections, especially those for optically forbidden transitions, to be highly accurate for incident energies above approximately 10 eV. However, it is qualitatively clear that these cross sections are small, and hence the accuracy requirements are expected to be low for practical applications. An interesting observation from this figure is the relatively large cross section for excitation of the $(3d^9 4s^2 4p)^1P^o$ state, i.e., the promotion of an inner 3*d*-electron. Note that cross sections for these inner-shell processes cannot be predicted by core-potential approaches with only two active target electrons accounted for.

B. Resonance analysis

Table III summarizes the resonance features identified in the BSRM calculations. These results were obtained by performing a time-delay analysis of the *S*-matrix elements, similar to what we did in our recent work on *e*-Ar collisions [13]. Note that the *R*-matrix method, as used in the present calculations for generating cross sections, does not provide a unique recipe for classification of the resonances. In order to get some indirect clues regarding the classification, we analyzed the channel expansion of the *R*-matrix poles in the vicinity of each structure. If appropriate, the largest contribution from the closed channels was then taken as the principal component of the resonance under consideration.

As can be seen from Table III, there is excellent agreement between the resonance positions predicted in the BSRM approach and the limited amount of experimental

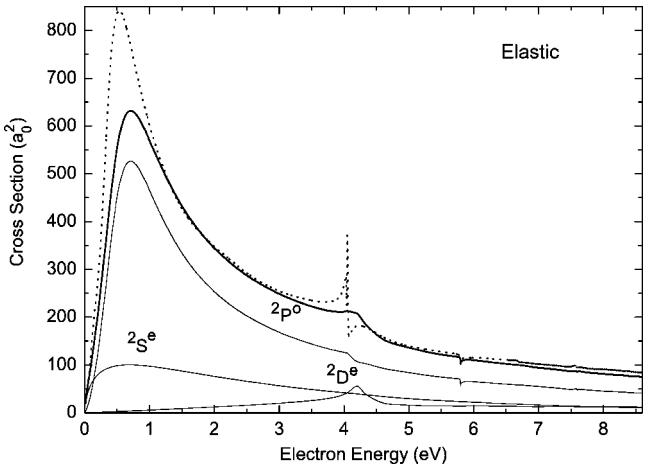

FIG. 2. Angle-integrated cross section (units of a_0^2) for elastic electron scattering from zinc atoms in their ground state $(4s^2)^1S$. The dashed line represents the core-potential results, while the thick solid line exhibits the predictions from the BSRM approach. The remaining thin solid lines show the most important partial-wave contributions, as obtained in the BSRM approach.

data available. One interesting feature is the region around the $(4s4p)^1P^o$ threshold just below 5.8 eV. Our time-delay analysis suggests that the structure in the cross section is *not* due to the $(4s4p^2)^2S$ resonance [8], but instead is a cusp effect associated with the opening of new channels. We also classify the features seen experimentally at 7.55 eV as the $(4s5p^2)^2D$ resonance and at 7.65 eV as $(4s4d5p)^2F^o$. These classifications differ from those given by Sullivan [8], but the latter authors explicitly labeled their assignments "tentative." due to the very limited experimental evidence. In principle, angle-resolved measurements could be used to either confirm or dispute our revised classification. Finally, we identify additional features that have not yet been classified experimentally, and we also provide the corresponding widths.

IV. SUMMARY AND CONCLUSIONS

Results for elastic scattering from and electron-impact excitation of Zn in its ground state $(4s^2)^1S$ were obtained using

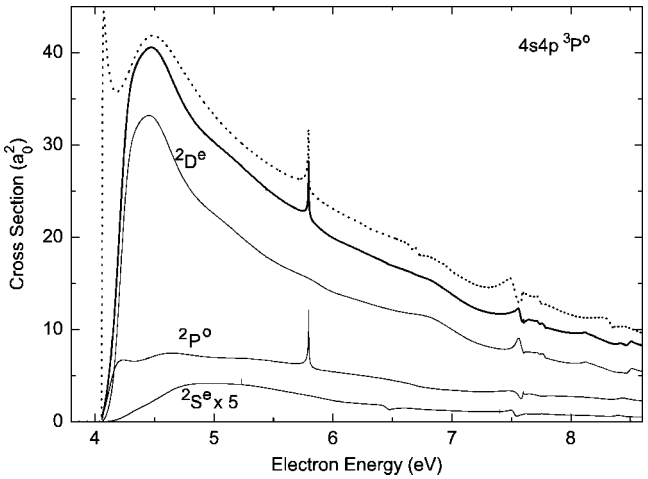

FIG. 3. Same as Fig. 2 for electron-impact excitation of the $(4s^2)^1S \rightarrow (4s4p)^3P^o$ transition.

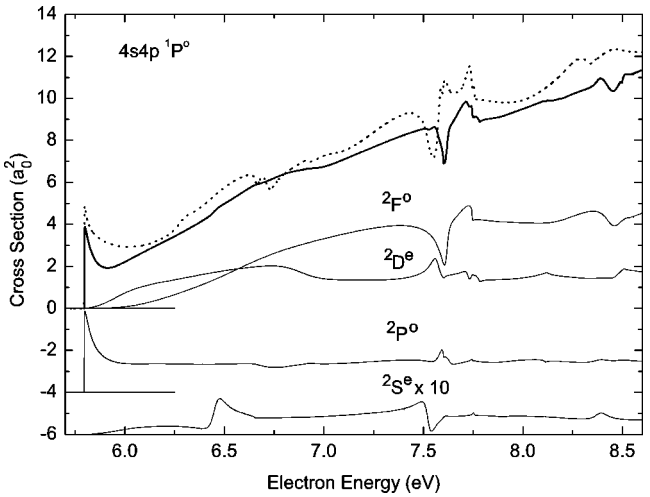

FIG. 4. Same as Fig. 2 for electron-impact excitation of the $(4s^2)^1S \rightarrow (4s4p)^1P^o$ transition.

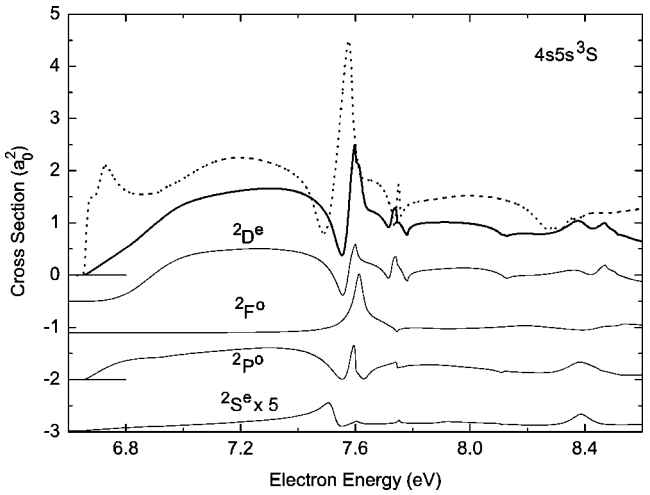

FIG. 5. Same as Fig. 2 for electron-impact excitation of the $(4s^2)^1S \rightarrow (4s5s)^3S$ transition.

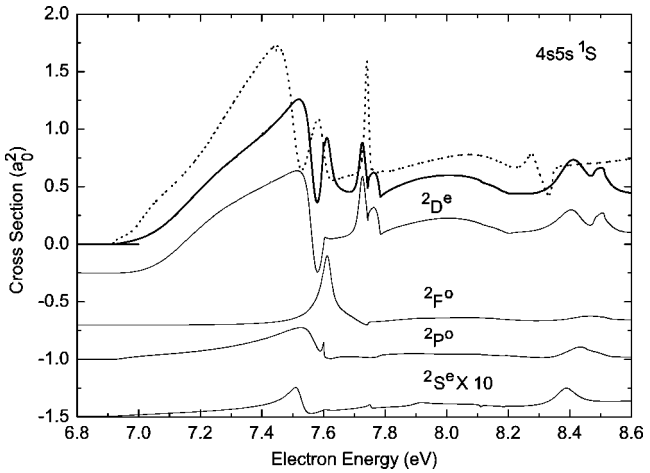

FIG. 6. Same as Fig. 2 for electron-impact excitation of the $(4s^2)^1S \rightarrow (4s5s)^1S$ transition.

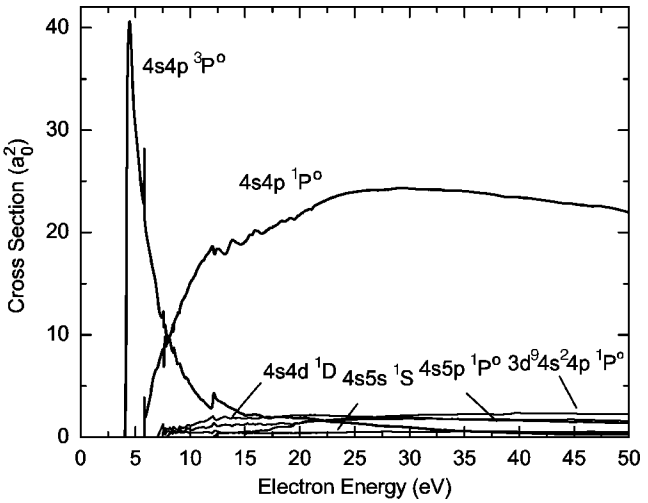

FIG. 7. BSRM cross sections (units of a_0^2) for electron-impact excitation of selected Zn states from the ground state $(4s^2)^1S$ as a function of the incident electron energy.

two independent theoretical approaches. The results were compared with each other and with the very limited experimental data available. Overall, both models yield satisfactory results, but the highly flexible *B*-spline *R*-matrix approach appears superior in the description of very fine details. At the present time, however, this method is most reliable only in the near-threshold regime. This limitation is particularly important for the description of optically forbidden transitions, where coupling to the target continuum is known to be important. This coupling can be accounted for in the *R*-matrix with pseudostates (RMPS) [21,22] and convergent close-coupling (CCC) approaches [23,24]. It can also be done in the BSRM method, but further development work is required in order to span the continuum with a relatively small number of pseudo-states. This development will keep the subsequent collision calculation tractable, requiring only modest computational resources such as desktop workstations.

However, since the cross sections for optically forbidden transitions fall off rapidly with increasing energy, a loss of accuracy in the computational method is not expected to be a major problem for modeling applications. Consequently, we expect the current results to fulfill the most urgent demands regarding data for *e*-Zn collisions. Electronic data files are available from the authors upon request.

TABLE III. Resonance parameters obtained in the BSRM model. Except if indicated otherwise, the experimental data and classifications are those given by Sullivan *et al.* [8].

Feature	Energy (eV)	Width (meV)	Experiment	
$(4s^2\varepsilon p)^2P^o$	0.707	1140	$(4s^2\varepsilon p)^2P^o$	0.49 [7] 0.67 [20]
$(4s4p^2)^2D$	4.234	372	$(4s4p^2)^2D$	4.25
Cusp	5.796		$(4s4p^2)^2S$	5.79
$(4s5s^2)^2S$	6.455	75	$(4s5s^2)^2S$	6.4
$(4s5p^2)^2S$	7.524	51		
$(4s5p^2)^2D$	7.570	51	$(4s4d^2)$	7.55
$(4s4d5p)^2P^o$	7.595	24		
$(4s4d5p)^2F^o$	7.615	30	$(4s5p^2)^2D$	7.65
$(4s4d5s)^2D$	7.725	24		
$(4s6s^2)^2S$	7.904	142		
$(4s5d6s)^2D$	8.122	45		
$(4s7s^2)^2S$	8.389	184		
$(4s5d6p)^2P^o$	8.425	83		
$(4s5d6p)^2F^o$	8.438	80		
$(4s5d7s)^2D$	8.483	48		

ACKNOWLEDGMENTS

The authors would like to thank Professor P.D. Burrow for sending some of his experimental data in electronic form. This work was supported by the United States National Science Foundation under Grants No. PHY-0244470 and No. PHY-0311161.

[1] R. P. McEachran and A. D. Stauffer, J. Phys. B **50**, 511 (1997).
[2] K. Bartschat, O. Zatsarinny, I. Bray, D. V. Fursa, and A. T. Stelbovics, J. Phys. B **37**, 2617 (2004).
[3] M. Born, J. Phys. D **34**, 909 (2001).
[4] M. Born, Plasma Sources Sci. Technol. **11**, A55 (2002).
[5] R. D. White, R. P. McEachran, R. E. Robson, M. T. Elford, and K. Bartschat, J. Phys. D **37**, 3185 (2004).
[6] R. P. McEachran and M. T. Elford, J. Phys. B **36**, 427 (2003).
[7] P. D. Burrow, J. A. Michejda, and J. Comer, J. Phys. B **9**, 3225 (1976).
[8] J. P. Sullivan, P. D. Burrow, D. S. Newman, K. Bartschat, J. A. Michejda, R. Panajotovic, R. P. McEachran, and S. J. Buckman, New J. Phys. **5**, 159 (2003).
[9] K. A. Berrington, W. B. Eissner, and P. H. Norrington, Comput. Phys. Commun. **92**, 290 (1995).
[10] O. Zatsarinny and C. Froese Fischer, J. Phys. B **33**, 313 (2000).
[11] O. Zatsarinny and K. Bartschat, J. Phys. B **37**, 2173 (2004).
[12] J. Bömmels, K. Franz, T. H. Hoffmann, A. Gopalan, O. Zatsarinny, K. Bartschat, M.-W. Ruf, and H. Hotop, Phys. Rev. A **71**, 012704 (2005).
[13] O. Zatsarinny and K. Bartschat, J. Phys. B **37**, 2173 (2004).
[14] C. E. Moore, *Atomic Energy Levels* (NSRDS-NBS 35, Washington, 1971); see also http://physics.nist.gov/cgi-bin/AtData/main_asd.
[15] K. Bartschat, *Computational Atomic Physics* (Springer, Heidelberg, 1996).
[16] D. Goebel, U. Hohm, and G. Maroulis, Phys. Rev. A **54**, 1973 (1996).

[17] See http://physics.nist.gov/PhysRefData/Handbook/Tables/zinctable3.htm.
[18] O. Zatsarinny and C. Froese Fischer, J. Phys. B **35**, 4669 (2002).
[19] V. M. Burke and C. J. Noble, Comput. Phys. Commun. **85**, 471 (1995).
[20] R. J. Zollweg, J. Chem. Phys. **50**, 4251 (1969).
[21] K. Bartschat, E. T. Hudson, M. P. Scott, P. G. Burke, and V. M. Burke, J. Phys. B **29**, 115 (1995).
[22] K. Bartschat, Comput. Phys. Commun. **114**, 168 (1998).
[23] I. Bray, D. V. Fursa, A. S. Kheifets, and A. T. Stelbovics, J. Phys. B **35**, R117 (2002).
[24] D. V. Fursa, I. Bray, and G. Lister, J. Phys. B **36**, 4255 (2003).